AIAA AVIATION Forum
5-9 June 2017, Denver, Colorado
23rd AIAA/CEAS Aeroacoustics Conference

Acoustic shock formation in noise propagation during ground run-up operations of military aircraft

Brent O. Reichman,[1] Kent L. Gee, [2] Tracianne B. Neilsen,[3] and S. Hales Swift[4]
Brigham Young University, Provo, UT, 84602

and

Alan T. Wall[5] and Hilary L. Gallagher[6]
Air Force Research Laboratory, Wright-Patterson Air Force Base, OH, 45433

J. Micah Downing[7] and Michael M. James[8]
Blue Ridge Research and Consulting, LLC, Asheville, NC 28801

A distinctive feature of many propagating, high-amplitude jet noise waveforms is the presence of acoustic shocks. Metrics indicative of shock presence, specifically the skewness of the time derivative of the waveform, the average steepening factor, and a new wavelet-based metric called the shock energy fraction (SEF), are used to quantify the strength and prevalence of acoustic shocks within waveforms recorded 10-305 m from a tethered military aircraft. The derivative skewness is more sensitive to the presence of the largest and steepest shocks, while the ASF and SEF tend to emphasize aggregate behavior of the entire waveform. These metrics are applied at engine conditions ranging from 50% to 150% engine thrust request, over a wide range of angles and distances, to assess the growth and decay of shock waves. The responses of these metrics point to significant shock formation occurring through nonlinear propagation out to 76 m from the microphone array reference position. Although these strongest shocks decay, the metrics point to continued nonlinear propagation in the far-field, out to 305 m. Many of these features are accurately characterized using a nonlinear propagation scheme based on the Burgers equation, but this scheme fails to account for multipath interference and significant atmospheric effects over the long propagation distances, resulting in an overestimation of nonlinearity metrics.

Nomenclature

ASF	=	Average steepening factor
C_v	=	Coefficient of variation
ETR	=	Engine thrust request
f	=	Frequency, Hz
MARP	=	Microphone array reference position
OASPL	=	Overall sound pressure level, dB re 20 μPa
p	=	Pressure
PDF	=	Probability density function

[1] Ph.D. Candidate, Dept. of Physics and Astronomy, N283 ESC, AIAA Student Member.
[2] Associate Professor, Dept. of Physics and Astronomy, N283 ESC, AIAA Senior Member.
[3] Part-Time Assistant Professor, Dept. of Physics and Astronomy, N283 ESC, AIAA Member.
[4] Postdoctoral Fellow, Dept. of Physics and Astronomy, N283 ESC, AIAA Member.
[5] Research Physicist, Battlespace Acoustics Branch, Air Force Research Laboratory, 2610 Seventh St., Bldg. 441, Wright-Patterson AFB, OH 45433, AIAA Member, AIAA Member.
[6] Biomedical Engineer, Battlespace Acoustics Branch, Air Force Research Laboratory, 2610 Seventh St., Bldg. 441, Wright-Patterson AFB, OH 45433, AIAA Member, AIAA Non-Member.
[7] Senior Scientist, 29 N Market St, Suite 700, AIAA Member.
[8] Senior Principal Engineer, 29 N Market St, Suite 700, AIAA Member.

r	=	Distance from the MARP, m
SEF	=	Shock energy fraction
σ_p	=	Standard deviation of the pressure waveform
$\sigma_{\partial p/\partial t}$	=	Standard deviation of the first time derivative of the pressure waveform
θ	=	Angle measured with respect to the aircraft nose
t	=	Time, s
WPS	=	Wavelet power spectrum, Pa^2/Hz

I. Introduction

One of the distinctive features visible in waveforms of supersonic jet noise is the presence of acoustic shocks or large sudden increases in pressure. These shocks are often associated with the auditory phenomenon called crackle [1-3] and thus serve as an additional source of annoyance within jet noise. The nature of these shocks and their evolution in the noise field is dependent on their physical properties and origins. Steepened waveforms exist near the source [3, 4], but it has also been shown that waveforms from full-scale aircraft continue to steepen and form shocks further away from the source due to nonlinear propagation [5-7]. One of the first indications that nonlinear propagation played a role in far-field effects was a lack of atmospheric absorption in the far field noticed by Pernet and Payne [8] and later by Morfey and Howell [9]. The steepening of waveforms and formation of shocks was also shown by Blackstock [5] to increase at locations further away from the jet noise source though his analysis did not incorporate atmospheric absorption. The presence of acoustic shocks in jet noise led to efforts to quantify waveform steepening, shock content, and crackle. One of the first attempts was performed by Ffowcs Williams *et al.* [10] and was based on the statistical measure of skewness of the pressure waveform distribution. Ffowcs Williams *et al.* defined a distinctly crackling waveform as having a skewness above 0.4. Since shocks may exist without affecting the skewness of the pressure waveform, defining crackle based on the skewness of the waveform leads to an insufficient definition [4]. Nevertheless, skewness-based criteria continue to be used. A better quantification of waveform steepening and shock content is needed as the ability to quantify the steepened nature of jet noise waveforms will enable a correct comparison of these important characteristics between measurement locations, across engine conditions, and among different experimental datasets.

Recent work in quantifying the steepening of a waveform has concentrated on the presence of large derivative values associated with shocks [11-13]. These efforts often rely on metrics calculated from the waveforms. Such metrics may evaluate the time-domain [14, 15] or frequency-domain [9, 16] characteristics of the waveform, and have been applied to full-scale [17] and laboratory-scale [18, 19] data. However, one of the issues that arises from the use of metrics is their interpretation. In many cases it is difficult to tell at what point a waveform has steepened sufficiently to qualify as a shock and when it has unsteepened enough to no longer be considered a shock. In addition, the numerical values associated with some metrics have been criticized as having little physical meaning, making it difficult to interpret results and compare between experiments.

Understanding of these steepening metrics has been enhanced recently by theoretical and experimental analyses. In model-scale work, Baars *et al* [3] have shown values for various metrics in the near-field of model-scale supersonic jet noise in an attempt to locate the source of the shock-like behavior. Others, including Muhlestein *et al*. [11] and Reichman *et al.* [12], have tried to quantify the connection between shock content and metrics through analytical derivations involving nonlinearly propagating initially sinusoidal signals. This recent work not only helps put context to values seen when comparing metrics, but also points to possible issues when comparing between experiments, e.g., relative sampling rates and extraneous noise characteristics.

Investigation into the shock-related metrics continues in this paper with an application to full-scale military aircraft noise measured over a large aperture. Time waveforms, associated spectra, and a wavelet analysis show steepening in waveforms continues as distance from the source increases. Metrics to be calculated and compared include the skewness of the first time-derivative of the pressure waveform, the average steepening factor, and a new wavelet-based metric called the shock energy fraction (SEF). This represents the first time the SEF wavelet analysis has been applied to military jet noise measurements. In addition, these analyses represent the first time a connection has been made between noise measured over such a large propagation distance—from geometric near field to the far field of a military aircraft. Finally, the far-field propagation of waveforms is numerically predicted, and the resulting waveforms, spectra, and nonlinearity metrics are compared with the measured ones.

II. Measurement setup

The dataset examined in this paper was collected at Edwards Air Force Base, September 5, 2013. The experiment has already been extensively described by James *et al.* [20], but pertinent details are given in this paper. Noise

measurements were taken as a tethered F-35A was cycled through power settings ranging from idle to 150% ETR, or maximum afterburner. Each engine condition was measured multiple times throughout the course of measurements. The 235 unique measurement locations, chosen in accordance with ANSI S12.75 [21], represent the largest full-scale dataset to date, with microphones located as close as 10 m from the shear layer out to 1220 m away from the microphone array reference position (MARP), located 6.6 m behind the nozzle. Microphones were arranged in either line arrays, parallel to the jet centerline, or in semi-circular arcs centered at the MARP. As most of the noise generated by supersonic jets is emitted from the turbulent mixing that occurs behind the jet, the MARP represents a rough estimate of source location for many frequencies of interest. For arcs at 38 m and beyond, arc spacing of 5° between microphones was used in the direction of peak radiation, between 120° and 160°.

The microphone locations within 38 m of the aircraft are shown in Fig. 1, with the aircraft also included and shown to scale. Microphone locations beyond 38 m are shown in later plots. In the areas of maximum acoustic pressure, 6.35 mm (1/4") microphones were used, with sampling rates of either 192 kHz or 204.8 kHz. At 305 m, in the forward direction, waveforms were captured at measurement locations from 0° to 40° and 60° to 80° using sound level meters. The meters recorded time-history Waveform Audio File Format (wav) files at a sampling rate of 51.2 kHz. Measurements were conducted between 3:00 and 9:00 AM local time, with temperature varying between 19.4°C and 23.1°C, relative humidity between 37.6% to 45.7%, and an average wind speed of 3.3 kts.

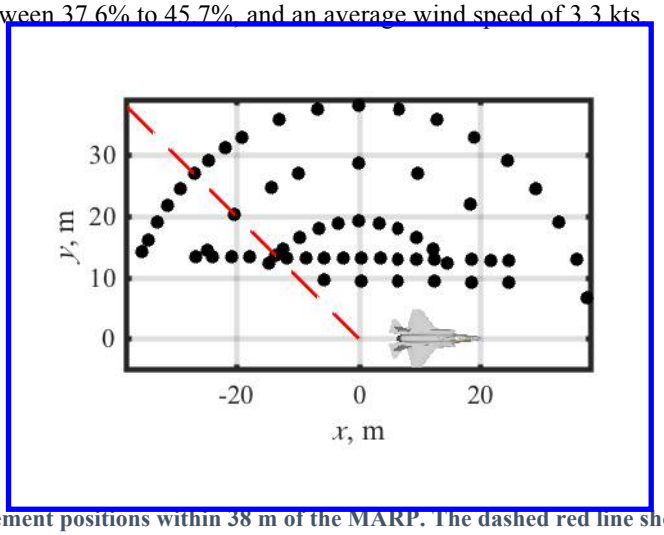

Fig. 1. Microphone measurement positions within 38 m of the MARP. The dashed red line shows the $\theta = 135°$ radial.

As an introduction to shock formation due to nonlinear propagation, normalized waveforms are considered (Fig. 2), at distances of 19, 29, 38, 76, and 152 m along the 135° radial, shown as a red line in Fig. 1. These waveforms are shown as a function of retarded time to demonstrate the evolution of waveform features with distance. Though some features do not align well between 19 m and 29 m due to near-field effects, at greater distances most features are preserved with respect to distance, indicating that this measurement radial is also a propagation radial. The most noticeable change occurs near 0.02 s, as the steepened portion of the waveform forms a distinct shock by 38 m from the MARP. This shock persists all the way out to 305 m, though it does decay slightly with respect to the rest of the waveform.

Though the largest shock is well-defined by 38 m from the MARP, nonlinear propagation continues to affect the waveform out to 152 m. In particular, smaller amplitude sections of the waveform, which are clearly not shock-like at 76 m, are significantly steeper at 152 m (around 0.01 s, for example), though they begin to slightly thicken by 305 m. Similar behavior was observed in the propagation of noise from another aircraft by Gee *et al*. [6] for a lower-power engine condition - the largest features steepen and form shocks by 38 m, but smaller-amplitude sections of the waveform continue to steepen beyond this distance. These waveforms show that shock formation within noise does not occur at a specific distance from the source but is a continuous process that is dependent on the amplitude and frequency content within each section of the waveform. To accurately characterize the nonlinear propagation and shock formation of entire waveforms, metrics are needed that express the steepness and shock characteristics of a waveform in a single value.

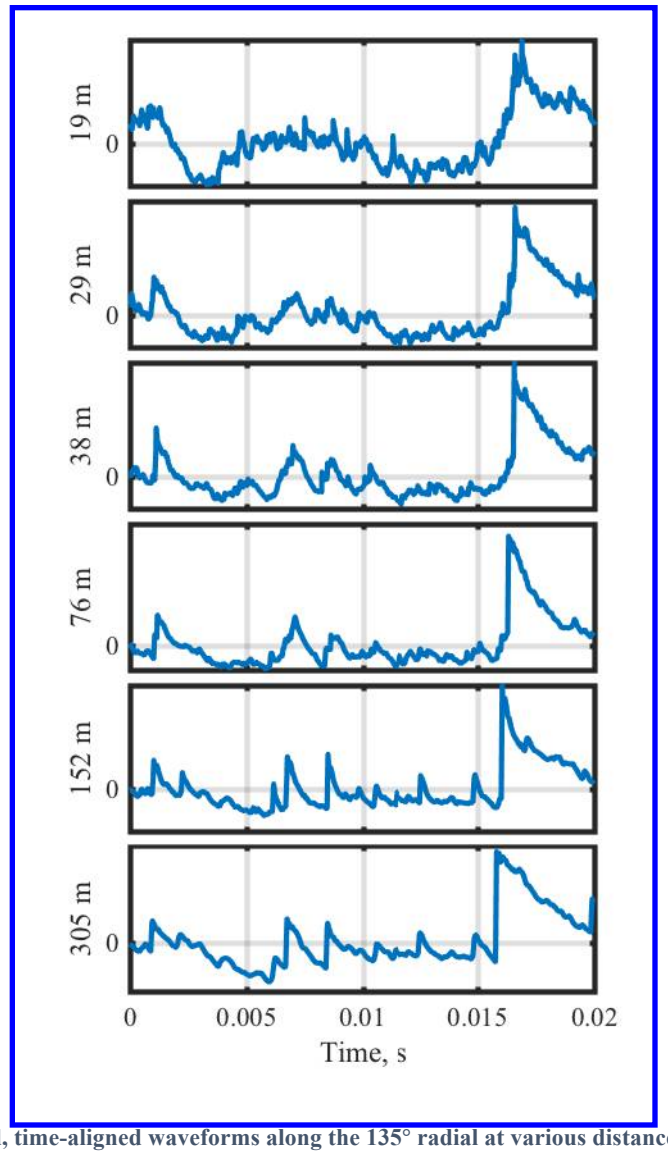

Fig. 2. Normalized, time-aligned waveforms along the 135° radial at various distances from the MARP.

III. Metrics indicative of nonlinear propagation

Because of the broadband, complex nature of nonlinear propagation and shock formation within jet noise, attempts to quantify the strength of shocks within jet noise have often concentrated on nonlinearity metrics, single values expressing the shock content of a waveform. Nonlinearity metrics considered in this paper are derivative skewness, ASF, and SEF, a new wavelet-based metric.

A. Derivative skewness

The skewness of the distribution of the first time derivative of the pressure waveform (estimated via finite difference) is a statistical measure that assesses the overall steepness of a waveform. Nonzero skewness values, generally, express an asymmetry in a distribution, and the large derivative values associated with acoustic shocks result in a distribution in which there are many slightly negative values with relatively fewer, but significantly larger positive values. This distribution results in a large positive derivative skewness indicative of steepened waveforms. Derivative skewness has been used to show the presence of shocks in both model-scale [13, 18] and full-scale [14, 22] analyses.

An advantage of this metric is that it is dependent only on the waveform shape and independent of an arbitrary definition of a shock, but it has notable disadvantages as well. First, sampling rate must be sufficient to adequately resolve the large positive derivatives associated with shocks and, hence, a relatively low sampling rate might cause the derivative skewness values to be severely underestimated [4, 12]. A physical interpretation of derivative skewness values has also proven difficult. Recent work [4, 12], however, has shown that a threshold of derivative skewness values of approximately 5 or larger indicates significant waveform steepening and shock content, provided that the sampling frequency exceeds the characteristic frequency in the waveform by a factor of at least 100.

B. ASF

Another time-domain metric that has been used to quantify waveform steepening is the average steepening factor (ASF), defined as the average value of positive derivatives divided by the average value of negative derivatives. This quantity was originally defined as the inverse, the waveform steepening factor $\mathrm{WSF} = 1/\mathrm{ASF}$ [23], and like the derivative skewness has been used in both model-scale [3] and full-scale [24] applications. A recent paper by Muhlestein *et al.* [11] derives analytical expressions for ASF for high-amplitude, initially sinusoidal signals, and additionally shows values for nonlinearly propagating noise in a plane-wave environment. A non-steepened waveform would have $\mathrm{ASF} = 1$, while steepened waveforms have higher values. Because the ASF is a linear mean of derivative values it represents trends within the entire waveform more than the derivative skewness, which accentuates the large positive outliers. However, the ASF is also more susceptible to the presence of extraneous noise than the derivative skewness [11, 12].

C. Shock energy fraction

The steepening of shocks in the time domain results in spectral broadening in the frequency domain, as energy is transferred from the peak frequency region to higher frequencies. Although this effect is often shown using the more familiar Fourier transform, a wavelet transform has been used in lab-scale jet noise analysis as a frequency-domain technique that also gives temporal resolution [3]. The wavelet analysis involves a convolution of the waveform with a wavelet shape to give spectral information that is time-resolved as well. The absolute value of this convolution, similar to a Fourier transform, may be squared to give the wavelet power spectrum (WPS), which if averaged over time approximates the autospectrum. Many types of wavelets exist, but for this paper the Morlet wavelet is used to mirror previous studies [3], where the wavelet analysis was used to show the association of high-frequency noise with shock waves and to investigate the near field of model-scale jet noise for evidence of shock wave origins [3]. An example of the wavelet transform applied to a waveform is shown in Fig. 3. The example waveform, of F-35A noise for 150% ETR at $r = 76$ m and $\theta = 135°$, is shown in Fig. 3(a) and has multiple shocks visible. The corresponding wavelet transform is shown in Fig. 3(b). In the WPS an increase in high-frequency energy is visible at times corresponding to rapid increases in pressure. This high-frequency energy in the WPS is indicative of acoustic shocks.

One metric involving the wavelet transform was proposed by Baars and Tinney [3]. This metric, a percent energy gain, used a shock detection algorithm to find sharp compressive regions of the waveform. Defining such sharp compressive regions using as a threshold derivative values above $\sigma_p/\Delta t$, where σ_p is the standard deviation of the pressure waveform and Δt is the time between samples, the algorithm identified the local waveform minima and maxima before and after these large derivative values to provide temporal bounds on the shock. Their algorithm then compiled an average spectrum of the WPS at the identified shocks. The average A-weighted spectrum of the shocks was then compared with the A-weighted spectrum of the entire waveform to determine the percent increase in energy due to the presence of shocks. This method has many interesting components, but a few shortcomings result in behavior that does not agree with expected shock behavior. One potential flaw in the percent energy gain was the application of the A-weighting to both the WPS and the waveform spectrum to correlate more closely with human perception. Though the A-weighting does serve to accentuate many of the highest frequencies, it may not have the desired effect in all situations. The shock detection algorithm was also shown in their paper [3] to be invalid for some propagation angles, which likely caused anomalous results. In addition, the spectral comparisons were performed based purely on the WPS, disregarding the number of shocks present in a waveform. This means that one shock within a 10-s waveform may be given the same emphasis as a waveform with 100 shocks per second.

To rectify these deficiencies, a new metric is proposed, the shock energy fraction (SEF). This metric bears many similarities to the percent energy gain, but with key differences. First, our shock detection threshold is based on $\sigma_{\partial p/\partial t}$, the standard deviation of the waveform derivative values to emphasize large derivative outliers common for shock waves while minimizing the effects of high-frequency noise that potentially contaminated the shock detection algorithm used previously [3]. A threshold of $15\sigma_{\partial p/\partial t}$ is set, and portions of the waveform with derivative values

above this threshold are considered to be shocks. Rather than compare spectra directly, a new approach is used that accounts for time in a manner similar to the sound exposure level (SEL) [25]; both the WPS and the duration of time associated with the number and length of shocks is used to define the SEF.

The primary difference in the WPS between the shock-containing portions and the remaining sections is the prominent presence of high-frequency sound, as seen in Fig. 3(b). The A-weighting applied in Ref. [3] minimized the effects of low-frequency noise, which remains consistent throughout the waveform and would otherwise dominate the higher-frequency differences that occur at a much lower decibel level. In contrast, the SEF is defined as an integral, not over the entire frequency range, but starting at a low-frequency limit. The justification for this lower-frequency limit can be seen in the coefficient of variation, c_v, shown in Fig. 3(c) as a function of frequency *f*. This coefficient is the normalized standard deviation of a function, $c_v = \sigma/\mu$, where σ is the standard deviation and μ is the mean value. Though ill-defined for many acoustics applications due to the abundance of zero-mean processes, C_v can be useful for energy-based applications (where explicitly non-negative values can be assumed) to show variation in a quantity. For the example waveform, C_v is shown to vary little below 1 kHz, and increases more rapidly above 2 kHz; C_v increases due to the large difference in WPS values between sections of the waveform with and without shocks. Using this as motivation, the WPS is integrated only above 2 kHz, roughly 10 times the peak frequency, to show the fraction of high-frequency energy associated with shock waves present in the waveforms.

With the above considerations, the SEF is defined as

$$\mathrm{SEF} = \frac{\sum_{t_{\mathrm{shocks}}} \sum_{f_{\mathrm{min}}=1\ \mathrm{kHz}}^{f_{\mathrm{max}}} \mathrm{WPS}\, \Delta f\, \Delta t}{\sum_{t} \sum_{f_{\mathrm{min}}=1\ \mathrm{kHz}}^{f_{\mathrm{max}}} \mathrm{WPS}\, \Delta f\, \Delta t}. \tag{1}$$

SEF is physically bounded between 0 and 1: SEF = 0 means that no high-frequency energy is found in the shocks, or that no shocks are observed, and SEF = 1 means that no high-frequency energy is observed outside of shock-containing regions of the waveforms. The behavior of SEF is compared to the derivative skewness and the ASF by application to the F-35 jet noise measurements described in Sec. II.

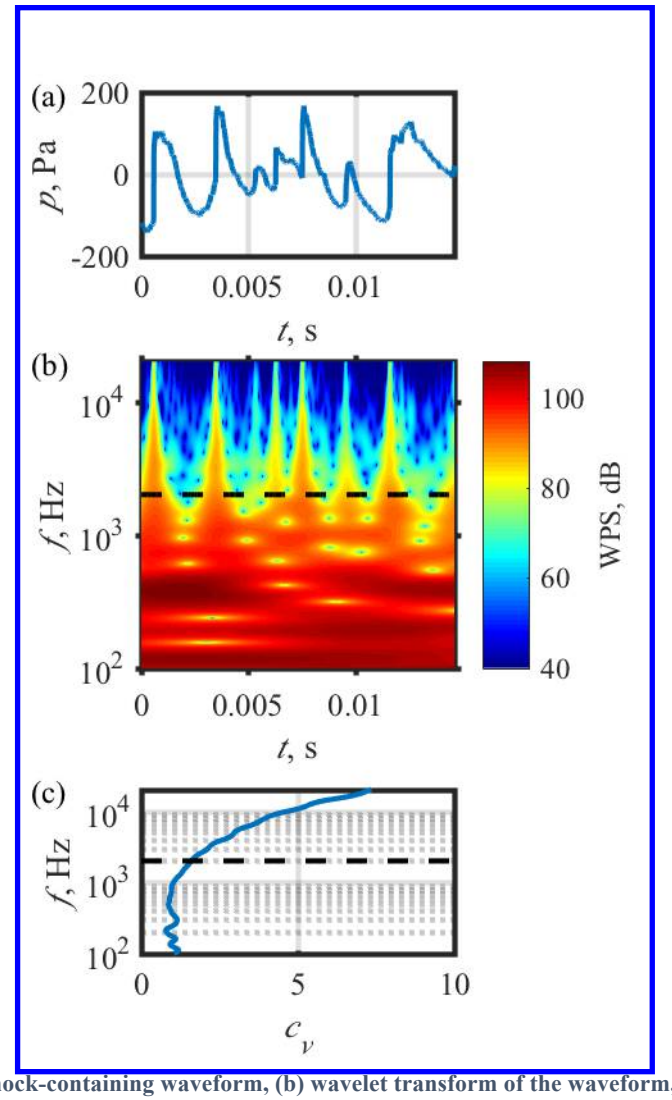

Fig. 3. An example (a) shock-containing waveform, (b) wavelet transform of the waveform, and (c) coefficient of variation for each frequency.

IV. Spatial trends

The shock quantification metrics introduced in Section III are shown over the entire measurement aperture in the this section. As the data were recorded at each engine condition multiple times, the average value between datasets is shown here, with five measurements at each engine condition. The results are shown at 50%, 75%, and 150% ETR. As the nozzle diameter is on the order of 1 m, the spatial map extends to roughly 300 nozzle diameters, farther than most laboratory-scale measurements [26, 27], though some far-field laboratory-scale measurements do exist [28].

A. OASPL

The directivity of jet noise and its dependency upon engine conditions are key features of jet aircraft noise as shown in Fig. 4 for 50%, 75%, and 150%. Microphone locations within 38 m of the MARP were shown in Fig. 1, and microphone locations at 76 m, 152 m, and 305 m are shown as black dots on the plot of the overall sounds pressure level (OASPL) in Fig. 4. More engine conditions may be seen in James *et al.* [20] for the F-35B, which is acoustically similar to the F-35A shown here [29]. In addition to the increase in OASPL seen at higher engine conditions, a shift in directivity is also observed. Whereas the OASPL peaks at 145° at 50% ETR, the directivity shifts forward, towards the nose of the aircraft, with increasing engine power. At 75% the OASPL peaks at 135° from the aircraft nose with the origin at the MARP, while at 150% it peaks at 125°. In all cases, the decay in the far field appears to be similar to the expected behavior due to geometric spreading, though this will be explored further in Section V.A.

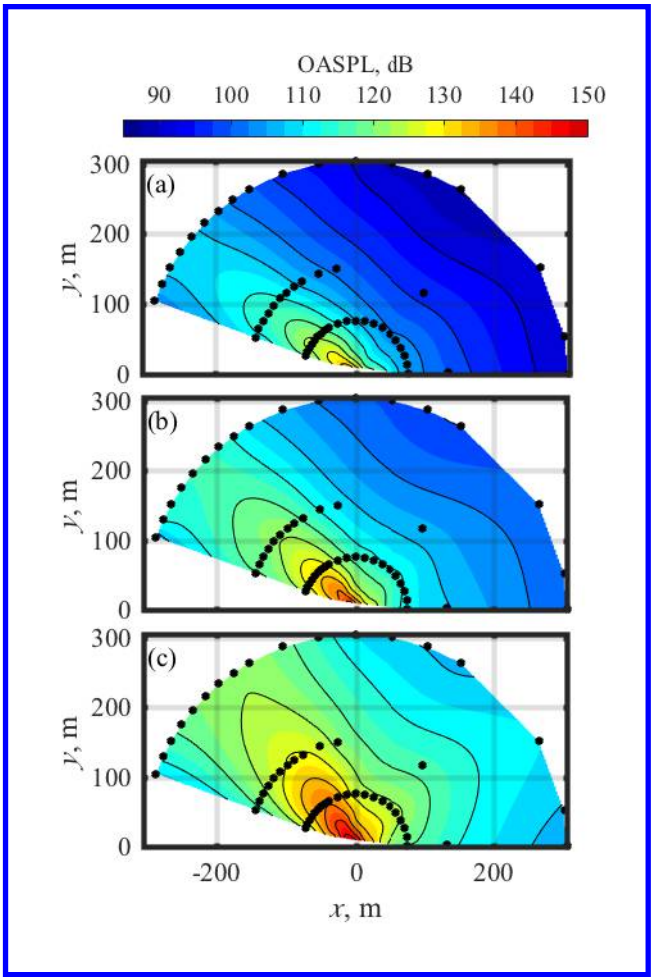

Fig. 4. OASPL near an F-35A at (a) 50% ETR, (b) 75% ETR, and (c) 150% ETR.

B. Derivative skewness

The presence and strength of acoustics shocks are readily shown by the derivative skewness, as evident in Fig. 5 at 50%, 75%, and 150% ETR. While the angular resolution of the data is every 5° in the peak radiation direction, the radial distribution in the far field is still rather coarse, with points at 76, 152, and 305 m, meaning that there are likely interpolation effects that accentuate the dip seen between 152 and 305 m, and more measurements are needed to precisely characterize the behavior. It is of note that some of the behavior seen between measurement locations in the far field of Fig. 5 is still in question. However, the measured behavior does indicate that at 150%, the derivative skewness decreases between 76 m and 152 m, then slightly increases between 152 m and 305 m.

The derivative skewness values shown in Fig. 5 are similar to those seen in prior studies. Similar values were shown for the F-35B in Ref. [20]. Some differences are seen when comparing the values at 50% and 150% with those reported by Gee *et al.* [4] for the F-35 AA-1. These difference are largely explained by the differences in sampling frequencies between the current study (196 or 204.8 kHz) and for the F-35 AA-1 study (96 kHz). When the waveforms from the current study are resampled the disagreements in large part disappear. For example, at 10 m from the MARP, the resampled derivative skewness is 5.5, in agreement with findings of Gee *et al.* At 38 m the resampled derivative skewness value drops from 22 to 16, still slightly elevated from the F-35 AA-1 result of 12, but with a much smaller difference between measurements.

Derivative skewness values depend on the engine power conditions. The derivative skewness values at 50%, shown in Fig. 5(a), are not indicative of the presence of shocks. The 50% ETR power condition derivative skewness peaks at a value of $\mathrm{Sk}\{\partial p/\partial t\} = 2.5$, below the threshold of ~5 that indicates significant shock content [12]. The near-field behavior of derivative skewness at 75% and 150% ETR differ greatly from that at 50%. Although not clear in the figure, at the closest measurement locations to the MARP along the direction of peak OASPL, the derivative skewness is approximately 7 or 8 for both 75% and 150% ETR. In both cases, the derivative skewness exceeds 20 at 76 m, and then decreases. This finding is in agreement with the behavior seen in Fig. 2, that the largest shocks are forming by

76 m from the MARP. However, important differences remain between 75% and 150% ETR. The derivative skewness reaches a slightly higher value at 150% of 27, compared with 25 at 75%. In addition, higher derivative skewness values persist over longer distances at 150%. At 305 m, the derivative skewness at 75% has dropped below a value of ten while it remains above 15 at 150%. Both of these values, while lower than the peak derivative skewness seen at 76 m, still indicate the presence of significant shocks in the jet's far field.

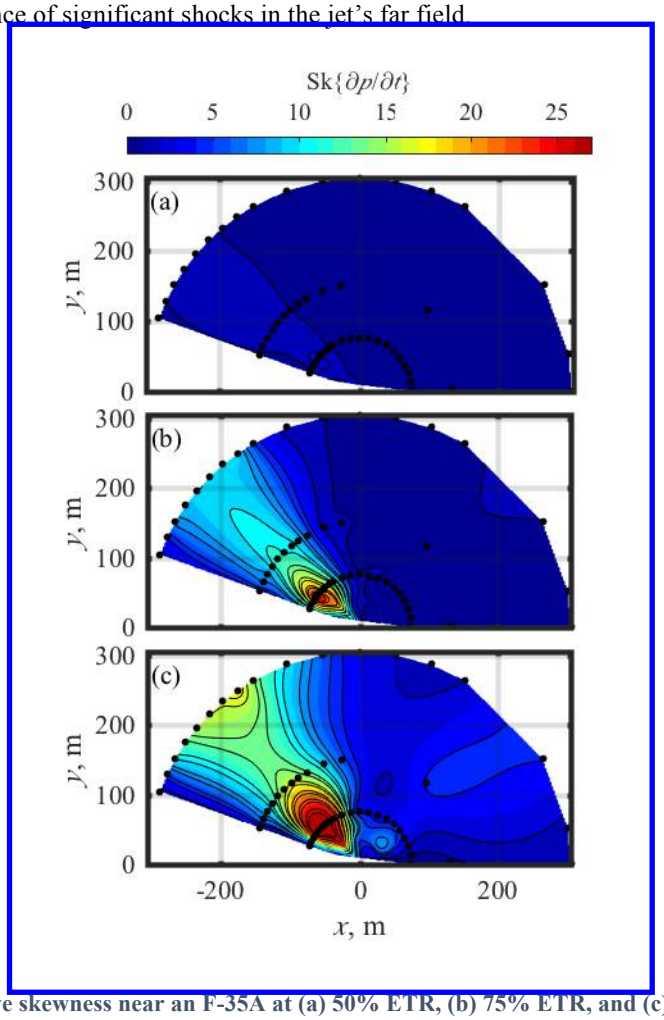

Fig. 5. Derivative skewness near an F-35A at (a) 50% ETR, (b) 75% ETR, and (c) 150% ETR.

C. Average Steepening Factor

While the derivative skewness accentuates the positive outliers and is likely to indicate the presence of the strongest shocks, the ASF is instead a measure of average behavior and thus, less sensitive to the less frequent but extremely large derivative values. Similar to the previous plots, at 50% ETR the low ASF values shown in Fig. 6(a) indicate that although the jet noise is steepening slightly, it does not contain shocks. However, at 75% the ASF (in Fig. 6(b)) reaches values above two in the direction of peak OASPL, indicative of more significantly steepened waves. In the analytical paper describing ASF by Muhlestein *et al.*, a value of 2 was reached by noise in a plane wave tube with a Gol'dberg number of $\Gamma = 3.3$. However, differences in the type of noise used by Muhlestein *et al*. affect ASF evolution, and our effective Gol'dberg number is likely higher than the direct comparison would suggest, based on the high derivative skewness values seen. The ASF is significantly higher at 150% ETR (in Fig. 6(c)), reaching values of 2.5. Since a value of ASF = 1 indicates a symmetric distribution of derivative values, a value of 2.5 is roughly 50% more than a value of 2. The peak ASF values are seen near the peak OASPL values, occurring at 140°, 130°, and 120° at 50, 75, and 150% ETR, respectively. These angles are slightly more forward than the OASPL peaks, in agreement with previously observed behavior [24].

Significant changes in behavior in the peak direction are seen between the three engine conditions. At 50%, a slight increase is seen through propagation away from the jet. At 75% the increase is much more dramatic, peaking at 76 m before decreasing out to 305 m. However, at 150% the ASF continues to increase along propagation radials even out to 305 m. Because the ASF represents a linear average of derivative values, it does not accentuate the largest shocks,

which cause the derivative skewness to peak at 76 m. The continually increasing ASF out to 305 m is due to continued nonlinear propagation, as seen by comparing the waveforms in Fig. 2. The nonlinear effects are evident in the combination of continued shock formation, general waveform steepening, and the persistence of shocks coupled with dissipation of high-frequency energy not associated with shocks due to atmospheric absorption. As designed, the ASF indicates the average strength of the shocks relative the overall signal; ASF continues to increase with distance as nonlinear propagation effects continue and atmospheric absorption reduces the lower-amplitude, high-frequency portions of the waveform.

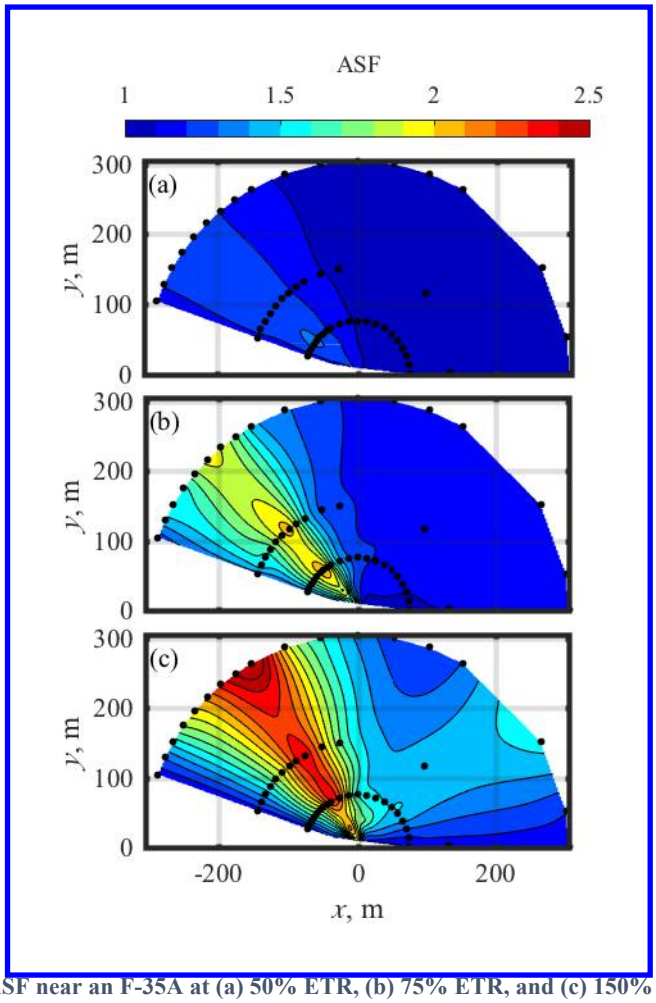

Fig. 6. ASF near an F-35A at (a) 50% ETR, (b) 75% ETR, and (c) 150% ETR.

D. Shock energy fraction

If the attenuation of high-frequency energy not associated with shocks is a cause of steadily increasing ASF values, this should be readily seen in the SEF, since the SEF shows the fraction of high-frequency energy (Above 1 kHz) associated with shocks. The SEF is examined over the spatial array, in Fig. 7, at 50%, 75%, and 150% ETR. In Fig. 7(a), the low SEF at 50% ETR again confirms the lack of significant shocks in the waveforms, though the values are non-zero in the direction of peak OASPL. Similar to the other metrics, a large change in metric behavior is seen when comparing 50% and 75% ETR. At 75% (Fig. 7(b)), the increasing prominence of shocks is evident as the SEF increases with distance to values above 0.1, meaning that the infrequent shocks contribute more than 10% of the energy above 1 kHz. At 75% ETR the SEF begins to decrease from 152 to 305m, but in contrast the 150% ETR in Fig. 7(c) continues to increase to 305 m, where it reaches values of above 0.12. These values suggest that the acoustic shocks are a main contributor of high-frequency energy at these distances from the source; high-frequency energy not associated with the shocks has likely been significantly attenuated due to atmospheric absorption. This attenuation is also seen when comparing the closest waveforms in Fig. 2 with those measured at farther distances. In addition, the growth in SEF with distance points to the persistence of nonlinear propagation and continued transfer of energy to higher harmonics. If nonlinear propagation were negligible, the SEF would remain constant or decrease as high-frequency energy is

absorbed at all sections of the waveform equally, similar to 50% ETR. Therefore, an increase in SEF points to continued nonlinear propagation out to 305 m from the MARP.

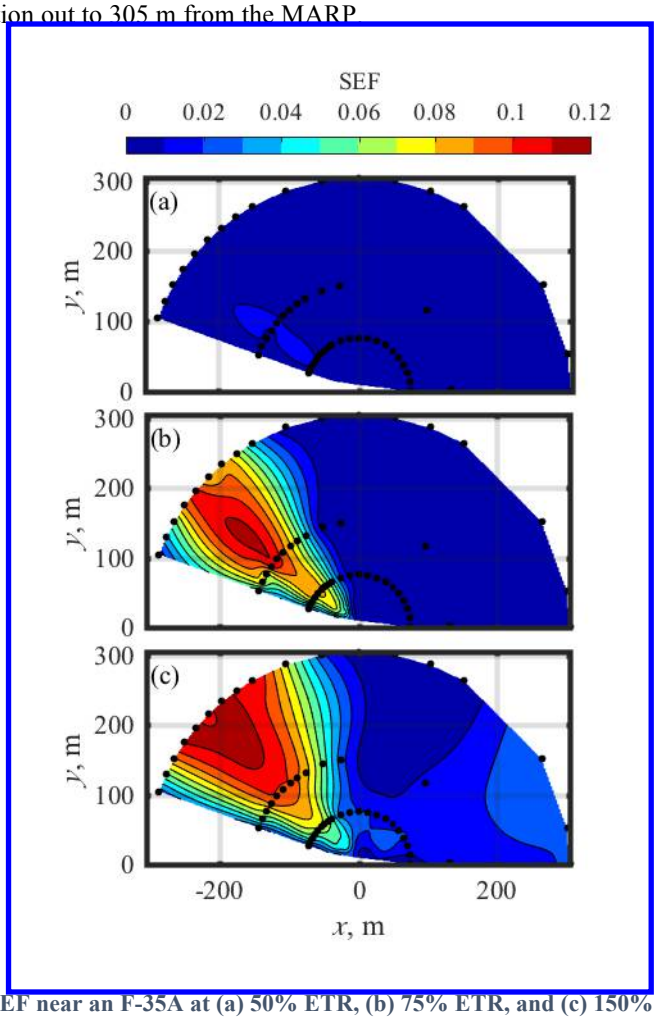

Fig. 7. SEF near an F-35A at (a) 50% ETR, (b) 75% ETR, and (c) 150% ETR.

E. Spatial trend summary

Though the above analyses all point to different aspects of shocks within jet noise, together they form a cohesive picture of continual nonlinear propagation away from the source of jet noise. All of the metrics suggest that the strongest shocks are not present immediately at the source but form through nonlinear propagation. The derivative skewness, emphasizing the largest positive outliers, peaks near 76 m, at which point the largest shocks have formed and begin decaying. However, because a noise signal is a complicated amalgamation of various frequencies rather than a simple sinusoid, shock formation is not limited to a particular spatial range. Though the largest shocks form by 152 m, overall waveform steepening and smaller shock formation continues to drive an increase in values of ASF. In addition, the rise in ASF is attributable to the decay in high-frequency energy not associated with shocks due to atmospheric absorption. This increase in the relative prominence of the shocks is also seen in the growth of SEF with distance. The evolution of these nonlinearity metrics over this large spatial aperture provides conclusive evidence that although some shocks exist in the near field of the jet noise source, the strongest acoustic shocks form by 76 m and nonlinear propagation persists out to at least 305 m from the MARP.

V. Nonlinearity metrics along radials

Though the spatial maps presented in Section IV are an efficient way to highlight trends associated with directivity and distance, there are advantages in considering propagation along individual measurement radials. Radial comparisons provide an easier way to see trends across engine conditions and show metric values at specific points

without interpolation effects. Such comparisons allows for inspection of specific features, such as the dip in derivative skewness seen in Fig. 5, as well as a more quantitative comparison of values between engine conditions. Presented in this section are plots of the metrics considered in Section IV as a function of distance along a single radial. These metric values are not from a single measurement, but an average of measurements throughout the experiment. The metric values are compared across engine condition and angle to establish and reinforce trends seen in the spatial maps, including the growth of the shocks near the jet source and continued shock formation and propagation into the far field.

A. Comparison across ETR

This section presents plots of the various metrics as a function of r for the same three engine conditions shown above. At each engine condition, the single radial displayed corresponds to the angle in the 305 m arc at which the greatest OASPL is measured. The angles of peak OASPL are 145°, 135°, and 125° at 50%, 75%, and 150% ETR respectively. The selected radial for 75% contains more measurements than 50% and 150, which accounts for the differences in the number of data points in the plots of derivative skewness, ASF and SEF shown in Fig. 8, as well as the OASPL in Fig. 8(a).

The derivative skewness displayed in Fig. 5 shows a marked peak at 76 m across all engine conditions. When each radial is inspected individually, as in Fig. 8(b), the same behavior is observed. Although the derivative skewness values at 50% do not suggest the presence of significant shocks, the 75% derivative skewness peaks at 76 m with a value of 20. After this point the derivative skewness decreases to 12 at 152 m and further decreases to 10 at 305 m. In contrast, the 150% derivative skewness peaks at 76 m with a value of 28, decreases to a value of 15 at 152 m, then rises again to 18 at 305 m. The slight increase again points to the importance of nonlinear propagation in the far field. Though the derivative skewness does not indicate the precise cause of the increase, three effects of nonlinear propagation are probably responsible: Shock formation, waveform steepening without forming distinct shocks, and the reduction in high-frequency noise not associated with shocks. A combination of these effects results in the increase in derivative skewness at 150% ETR.

Many of the trends observed in the plots of the derivative skewness are again reinforced when considering the ASF. As shown in Fig. 8(c), the ASF peaks for 50% and 75% ETR at 76 m, similar to the derivative skewness. And, similar to the derivative skewness, the ASF at 75% ETR decreases consistently after 76 m, which is different than the behavior seen at 150%. The ASF at 150% ETR continues increasing with distance, from a value of 2.2 at 76 m to a value of 2.5 at 305 m. This continued increase with distance again points to nonlinear propagation in the far field of military jet aircraft.

The continued increase of ASF out to 305 m is in part due to absorption of high-frequency noise not associated with acoustic shocks. At closer distances, this "background" high-frequency noise creates large positive and negative derivatives that lower both the derivative skewness and ASF below what examination of the shock content in the waveform suggests. However, as this high-frequency energy propagates and is attenuated through atmospheric absorption, the remaining shocks are accentuated in both the derivative skewness and the ASF.

The attenuation of high-frequency energy is apparent in plots of the SEF, shown in Fig. 8(d). The SEF at 50% remains more or less constant, while at 75% and 150% SEF grows with distance to 152 m. At 75%, SEF decreases slightly from 152 m to 305 m; this decrease is associated with a decrease in the number of shocks. However, at 150% the SEF is, like the ASF in Fig. 8(c)**Error! Reference source not found.**, increasing with distance out to 305 m, confirming the reduction in high-frequency energy not associated with shocks. One point to mention is that the SEF is higher at most distances for 75% than 150%. The exact cause of this discrepancy is unknown, but it is likely due to a combination of effects, including different directivity at the two engine conditions, the number of shocks, and difference spectral content.

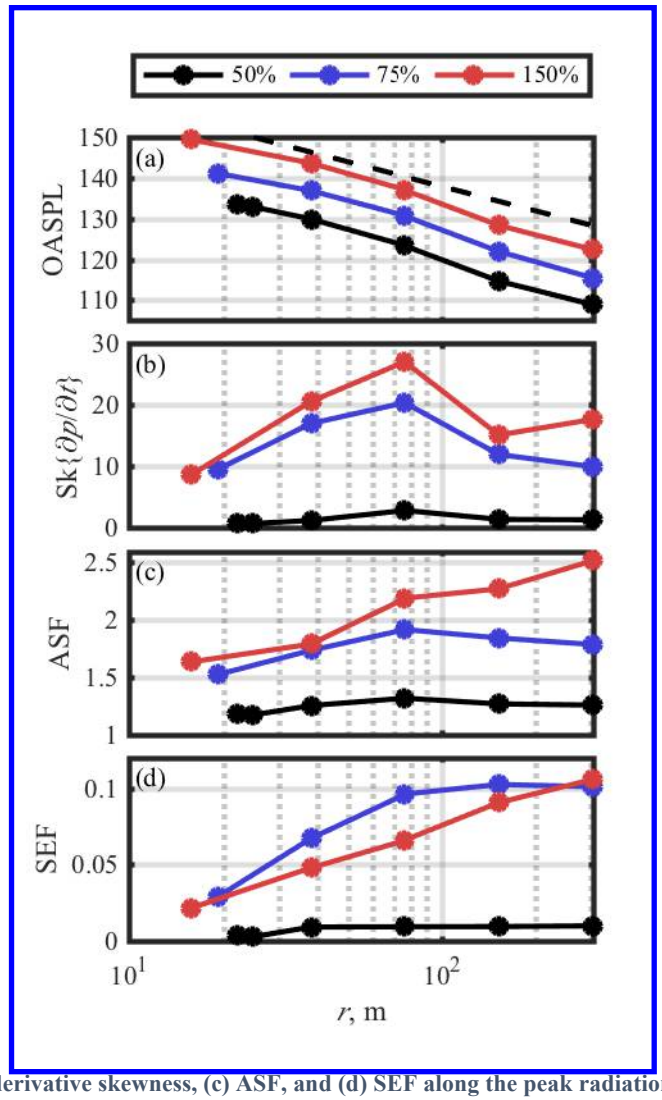

Fig. 8. The (a) OASPL, (b) derivative skewness, (c) ASF, and (d) SEF along the peak radiation angle at 50%, 75%, and 150% ETR.

B. Angular dependence of nonlinearity metrics

Some of the behavior seen in the line plots of nonlinearity metrics, in particular the fall and subsequent rise in derivative skewness seen in Fig. 8, raise the question as to whether the effects are physical or merely the result of a single microphone with a poor response or signal-to-noise ratio. To show that the trends observed in Section V.A are physical, the metrics are plotted for various angles at 150% ETR in Fig. 9; the OASPL, derivative skewness, ASF, and SEF are plotted as a function of r for the microphones along the 120°, 130°, 140°, and 150° radials.

The OASPL shown in Fig. 9(a) decays close to the rate expected due to spherical spreading. This rate, 20 dB/decade or 6 dB/doubling of distance, is seen between most points. However, there is one discrepancy: all radials decrease by 8-9 dB between 76 m and 152 m. It is likely that this discrepancy is mostly due to meteorological effects, though some decrease in amplitude is also expected due to nonlinear effects. Between 152 m and 305 m the decay is again roughly equal to 6 dB across all radials. This shows that nonlinear propagation has an important effect, not only on the spectrum or presence of shocks but on the OASPL, which must be taken into account in the far field.

Behaviors observed in Section V.A are shown in Fig. 9 to occur across multiple angles. The derivative skewness, shown in Fig. 9(b), does experience a large decrease between 76 m and 152 m, likely due to the attenuation of the largest shocks that also causes the added decrease in OASPL. However, between 152 m and 305 m the derivative skewness either remains constant or increases across all angles in question. This points to the likelihood that past 152 m there is continued steepening and nonlinear propagation continues to play an important role.

The ASF and SEF again confirm this continued waveform steepening and importance of nonlinear propagation well into the far field of the jet noise source. Across all angles, the ASF and SEF continue to increase out to 305 m.

Because they are not as sensitive to large outliers, they do not experience the decrease between 76 m and 152 m seen in the derivative skewness, but rather emphasize the continued steepening and presence of high-frequency energy associated with nonlinear propagation.

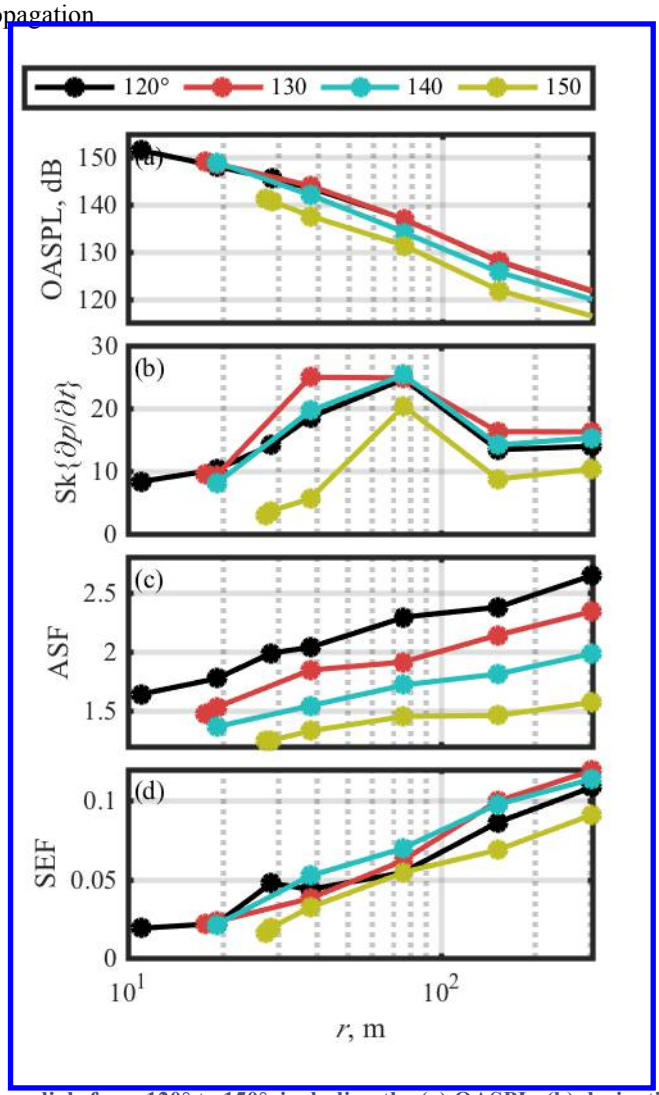

Fig. 9. Various metrics along radials from 120° to 150°, including the (a) OASPL, (b) derivative skewness, (c) ASF, and (d) SEF at 150% ETR.

VI. Numerical Modeling

Although the behavior discussed above accurately characterizes many aspects of nonlinear propagation within jet noise, spatial resolution is limited in the far-field. In order to gain more information about waveform evolution between and beyond measurement points, the nonlinear propagation can be modeled using numerical tools. Nonlinear propagation, including the formation and decay of shock waves in complex signals, can be accurately predicted using numerical algorithms [30, 31]. Blackstock [5] was one of the first to attempt to predict nonlinear propagation of jet noise, followed by Morfey and Howell [9]. Predictions of nonlinear behavior have been shown for multiple aircraft [6, 30, 32, 33], including the F-35 [20]. Many of these algorithms are based on the generalized Burgers equation (GBE), which accounts for quadratic nonlinearity in an arbitrary waveform while also incorporating atmospheric absorption and geometric spreading. These algorithms have been shown to accurately capture many aspects of the pressure waveform, in addition to spectral effects due to nonlinear propagation [29, 30]. A hybrid time-frequency domain algorithm is used; the same model was used by Reichman *et al*. [29] to model spectral changes due to nonlinear propagation. That paper successfully showed the influence of nonlinear propagation for high-frequency energy in the far field of an F-35B, in particular in a comparison between measured data and linear and nonlinear predictions. Though low-frequency (below 1 kHz) agreement was questionable due to multipath interference effects, an empirical

correction based on low-amplitude propagation was applied to provide agreement over the whole spectral range. The comparison between nonlinear and linear predictions showed the large impact nonlinear propagation has on high-frequency energy within jet noise and showed that nonlinear propagation algorithms can accurately characterize those effects.

The prediction of nonlinearity metrics using nonlinear propagation algorithms has yet to be explored in depth. Due to the metrics' sensitivity to small changes in derivative values, and in particular to shock amplitude, comparing nonlinearity metrics between numerically propagated data and measurements will help evaluate the robustness of the numerical algorithms. By improving upon these algorithms in the future, measurements closer to the aircraft will be able to more accurately characterize effects seen during long-range propagation away from the aircraft.

A. Waveform characteristics

The ability of models to capture realistic propagation can be shown by comparing the waveforms themselves and their characteristics, as shown in Fig. 10 for a segment of a measured (black) and a numerically propagated (red) waveform. The simulated waveform was obtained by numerically propagating the waveform measured at 76 m to 305 m using the GBE code. This code includes important effects such as geometric spreading, atmospheric absorption, and quadratic nonlinearity. However, other effects not taken into account include atmospheric turbulence and multi-path interference, such as reflections from the rigid ground or from a downward-refracting atmosphere. These discrepancies may have a noticeable effect on the time waveforms and spectral characteristics.

Despite propagation effects that are not considered, many features of the waveforms shown in Fig. 10(a) align closely with each other. The waveforms are time-aligned using a cross-correlation and while there are some discrepancies between the waveforms, the largest shocks and other significant features align closely.

Some of the discrepancies between the measured and propagated waveforms are more evident in the PDFs of the waveform derivative values, plotted in Fig. 10(b) as a function of the standard deviation of the derivative values, $\sigma_{\partial p/\partial t}$. Because the numerical simulation assumes an ideal atmosphere, many of the largest positive derivative values, near $50\sigma_{\partial p/\partial t}$, are higher in the numerical case than in the measured data. However, one of the largest differences occurs in the negative derivatives. The numerical propagation algorithm entirely eliminates larger negative derivative values, while the negative values in the measurement, while not as large as the positive derivative values, are significantly larger than the numerical case. This difference is likely due to the ideal-atmosphere assumptions in place in the numerical propagation, and are present in the waveform as slightly noisier signals, in particular away from the shocks.

These differences in the waveforms and PDFs have little effect on the spectra shown in Fig. 10(c). Some disagreement is seen in the low-frequency regime due to multi-path interference effects. Though this discrepancy can be empirically corrected in the frequency domain [29], the focus of this paper is time-domain features, which are more difficult to correct for such effects. Above 400 Hz, both spectra agree remarkably well. This is due to the large amount of high-frequency energy associated with shocks, as evidence by the large SEF values, which dwarf smaller effects throughout the rest of the waveform. Though there are some differences, the numerical propagation accurately captures many of the aspects of nonlinear propagation, including the shocks present in the waveforms and the spectra.

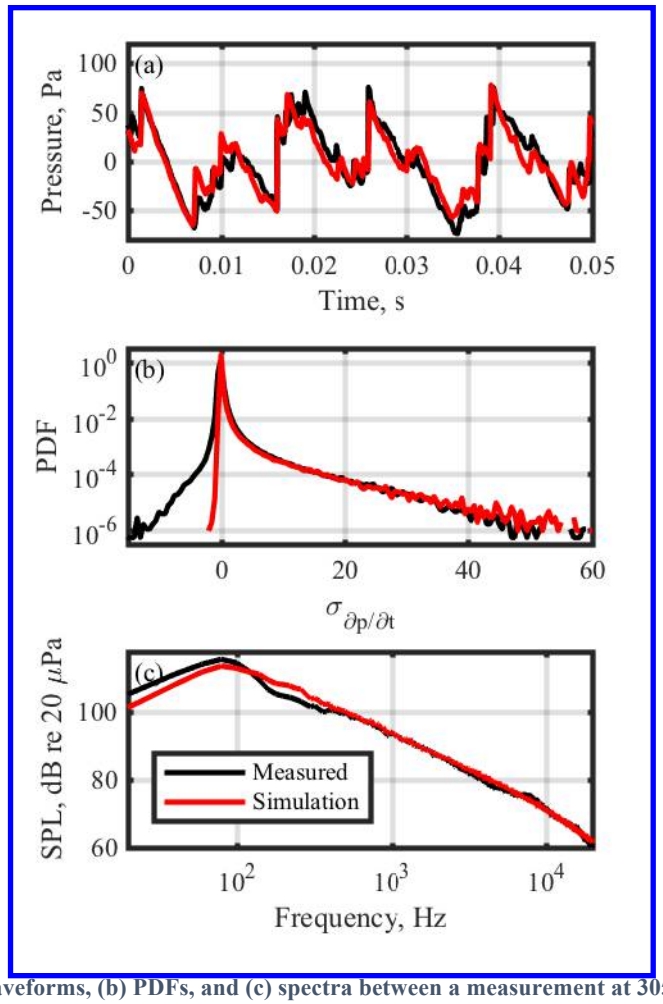

Fig. 10.Comparison of (a) waveforms, (b) PDFs, and (c) spectra between a measurement at 305 m and data numerically propagated from 76 m to 305 m.

B. Prediction of Nonlinearity Metrics

The differences in the derivative PDFs in Fig. 10(b) are likely to play an important role in accurately predicting the evolution of the nonlinearity metrics previously discussed. In particular, the lack of large negative derivative values affects both the derivative skewness and the ASF of the numerically propagated waveform at distances between 76 m and 305 m. These values, in addition to the metric values calculated from the measured waveforms, are shown in Fig. 11. In the case of derivative skewness, the lack of large negative derivative values in the propagated waveform causes an almost immediate jump, after which the values decrease steadily out to 305 m. In the case of ASF, the lack of large negative derivatives becomes more apparent with distance as all initial high-frequency energy not associated with shock waves is linearly attenuated in the propagated waveform. This overestimation of nonlinearity metrics points to the need for improved, more realistic long-range atmospheric propagation models, including multi-path interference effects that are likely to decrease time-domain metric values (See Appendix A). Though the current Burgers equation code accurately predicts many of the waveform characteristics, including steepening and increased high-frequency energy associated with shock formation, more accurate propagation modeling is needed to accurately predict other features of the waveforms.

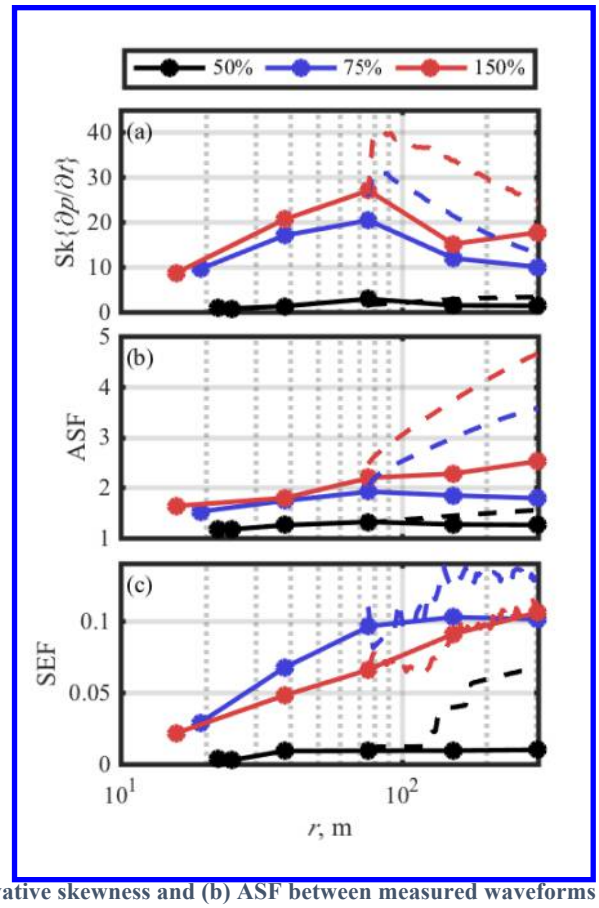

Fig. 11.Comparison of (a) derivative skewness and (b) ASF between measured waveforms and numerically propagated waveforms.

VII. Conclusions

The various nonlinearity metrics considered in this paper point to the conclusion that nonlinear propagation is an important factor in the near, mid, and far-field environments of military jet noise. Though some significant shocks exist at the closest measurement locations roughly at a distance of 10 m, the waveforms steepen and form shocks through nonlinear propagation. The nonlinearity metrics indicate that the strongest shocks form by 76 m then decay. This growth and decay of the strongest shocks is shown by increasing then decreasing derivative skewness values; the reduction in OASPL—2-3 dB more attenuation than expected due to spherical spreading and atmospheric absorption between 76 m and 152 m—supports this claim. The continued growth of ASF points to nonlinear propagation out to at least 305 m, likely due to the persistent steepening of lower amplitude features in the noise. The wavelet-base metric SEF appears to be a useful nonlinearity metric. For the F-35, the increase in SEF with distance indicates that high-frequency energy not associated with shocks is attenuated through linear atmospheric absorption.

The continued importance of nonlinear propagation in assessing far-field effects of jet noise is confirmed through numerical modeling. Using a numerical propagation scheme based on the Burgers equation, characteristics of the waveform and spectra are accurately predicted. However, important differences between the measured and propagated waveforms cause an overestimation of nonlinearity metrics, pointing to the need for more advanced modeling schemes that take into account complex atmospheric effects.

Appendix A. Ground Reflection Analysis

One of the complications of military jet noise measurements is the presence of a rigid ground. This complication, which is not present in model-scale measurements typically performed in an anechoic chamber, results in multi-path interference effects. Though these multi-path interference effects are often manifest in the frequency domain, they also have a noticeable effect on nonlinearity metrics. These effects make accurate numerical propagation difficult, as

all measurement points are contaminated with ground reflections, and measurement points along the same radial usually have different interference patterns.

Because measured jet noise contains ground-reflected noise, a numerical case study is performed to assess the effects of multiple paths on nonlinearity metrics. In this study, a random Gaussian waveform is filtered to have an OASPL and frequency content similar to the jet noise at 38 m and 135°, sans interference nulls. This waveform is then numerically propagated using the GBE algorithm to different measurement locations, allowing shocks to form and decay. Assuming perfect coherence between the direct and indirect path and a perfectly rigid ground, the waveform is propagated as if reflecting off the ground to the measurement locations. The direct and reflected waveforms are combined and nonlinearity metrics are calculated. In this simulation, both the direct source and measurement locations are located 2.5 m above the ground. The original wave and the reflected wave (at 38 m) are added then numerically propagated from 38 m to 125 m. An example of the waveforms at 76 m is shown in Fig. A1 with and without inclusion of the ground reflected path. Although many of the overall features of the two waveforms are similar, the differences are likely to cause significant changes in nonlinearity metrics.

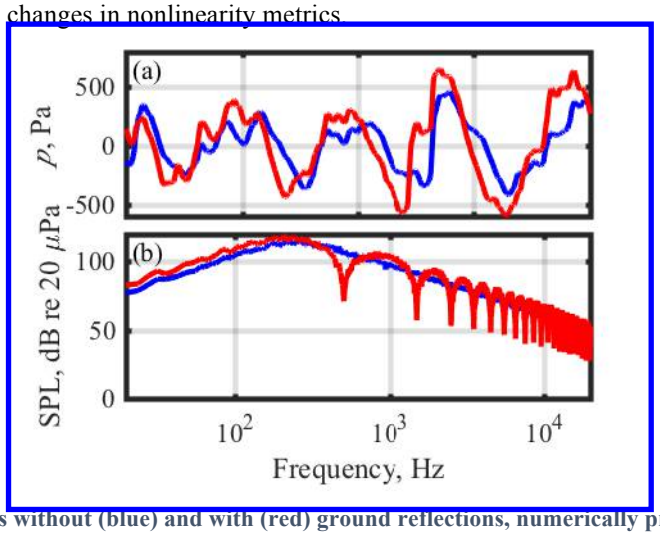

Fig. A1. Waveforms without (blue) and with (red) ground reflections, numerically propagated to 76 m.

The addition of the ground reflection interference in the input waveform induces a reduction in many time-domain nonlinearity metrics of the propagated waveform. The derivative skewness and ASF, shown in Fig. A2(a) and A2(b), are significantly reduced by the presence of a ground reflection. Interestingly, the presence of a ground reflection reduces the derivative skewness by an almost constant factor of near 30% once significant shocks have formed. While this difference alone is not enough to explain the large differences in derivative skewness seen in Fig. 11(a), it is a significant effect that must be taken into account to accurately predict the evolution of nonlinearity metrics. The ground reflection does not cause as dramatic an effect on the ASF, though the effect does grow with distance, leading up to a reduction of nearly 20%. Interestingly, the SEF, shown in Fig. 11(c), is not significantly affected by the presence of ground reflections. This analysis, while limited to one case study, shows that the presence of ground reflection in outdoor measurements likely decreases the derivative skewness and ASF.

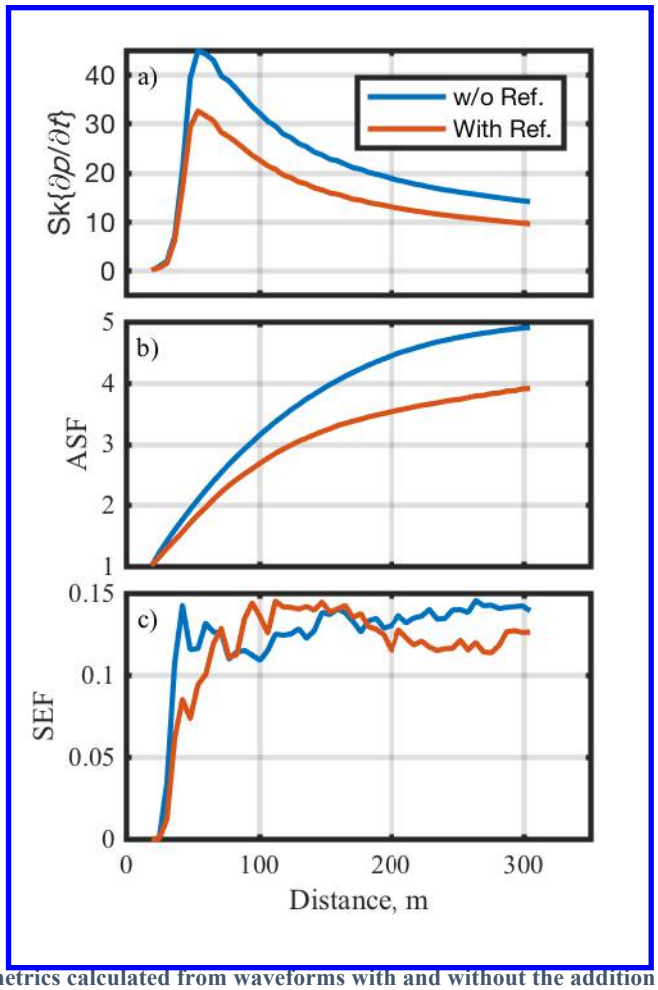

Fig. A2. Nonlinearity metrics calculated from waveforms with and without the addition of a ground reflection.

Acknowledgments

The authors gratefully acknowledge funding for the measurements, provided through the F-35 Program Office and Air Force Research Laboratory. (Distribution A: Approved for public release; distribution unlimited) B.O. Reichman was funded through by an appointment to the Student Research Participation Program at the U.S. Air Force Research Laboratory, 711th Human Performance Wing, Human Effectiveness Directorate, Warfighter Interface Division, Battlespace Acoustics Branch administered by the Oak Ridge Institute for Science and Education through an interagency agreement between the U.S. Department of Energy and USAFRL.

References

1. Krothapalli, A., Rajkuperan, E., Alvi, F., and Lourenco, L. "Flow field and noise characteristics of a supersonic impinging jet," *Journal of Fluid Mechanics* Vol. 392, 1999, pp. 155-181.

2. Gee, K. L., Sparrow, V. W., Atchley, A. A., and Gabrielson, T. B. "On the perception of crackle in high-amplitude jet noise," *AIAA Journal* Vol. 45, No. 3, 2007, pp. 593-598.

3. Baars, W. J., and Tinney, C. E. "Shock-structures in the acoustic field of a Mach 3 jet with crackle," *Journal of Sound and Vibration* Vol. 333, No. 12, 2014, pp. 2539-2553.

4. Gee, K. L., Neilsen, T. B., Wall, A. T., Downing, J. M., James, M. M., and McKinley, R. L. "Propagation of crackle-containing jet noise from high-performance engines," *Noise Control Engineering Journal* Vol. 64, No. 1, 2015, pp. 1-12.

5. Blackstock, D. T. "Nonlinear propagation of jet noise," *Third Interagency Symposium on University Research in Transportation Noise*. U.S. Department of Transportation, University of Utah, Salt Lake City, Utah, 1975, pp. 389-397.

6. Gee, K. L., Sparrow, V. W., James, M. M., Downing, J. M., Hobbs, C. M., Gabrielson, T. B., and Atchley, A. A. "The role of nonlinear effects in the propagation of noise from high-power jet aircraft," *The Journal of the Acoustical Society of America* Vol. 123, No. 6, 2008, pp. 4082-4093.

7. Mora, P., Heeb, N., Kastner, J., Gutmark, E. J., and Kailasanath, K. "Impact of heat on the pressure skewness and kurtosis in supersonic jets," *AIAA Journal* Vol. 52, No. 4, 2014, pp. 777-787.

8. Pernet, D. F., and Payne, R. C. "Non-linear propagation of signals in airs," *Journal of Sound and Vibration* Vol. 17, No. 3, 1971, pp. 383-396.

9. Morfey, C. L., and Howell, G. P. "Nonlinear propagation of aircraft noise in the atmosphere," *AIAA Journal* Vol. 19, No. 8, 1981, pp. 986-992.

10. Ffowcs-Williams, J. E. S., J.; Virchis, V.J. "'Crackle': an annoying component of jet noise," *Journal of Fluid Mechanics* Vol. 71, No. 2, 1975, pp. 251-271.

11. Muhlestein, M. B., Gee, K. L., Neilsen, T. B., and Thomas, D. C. "Evolution of the average steepening factor for nonlinearly propagating waves," *The Journal of the Acoustical Society of America* Vol. 137, No. 2, 2015, pp. 640-650.

12. Reichman, B. O., Muhlestein, M. B., Gee, K. L., Neilsen, T. B., and Thomas, D. C. "Evolution of the derivative skewness for nonlinearly propagating waves," *Journal of the Acoustical Society of America* Vol. 139, No. 3, 2016, pp. 1390-1403.

13. Baars, W. J., Tinney, C. E., Wochner, M. S., and Hamilton, M. F. "On cumulative nonlinear acoustic waveform distortions from high-speed jets," *Journal of Fluid Mechanics* Vol. 749, 2014, pp. 331-366.
doi: doi:10.1017/jfm.2014.228

14. McInerny, S., Downing, M., Hobbs, C., James, M., and Hannon, M. "Metrics that characterize nonlinearity in jet noise," *17th International Symposium on Nonlinear Acoustics*. Vol. 838, AIP Publishing, 2005, pp. 560-563.

15. McInerny, S. A. "Launch vehicle acoustics. II-Statistics of the time domain data," *Journal of aircraft* Vol. 33, No. 3, 1996, pp. 518-523.

16. Gee, K. L., Atchley, A. A., Falco, L. E., Gabrielson, T. B., and Sparrow, V. W. "Bispectral analysis of high-amplitude jet noise," *AIAA paper* Vol. 2937, 2005, p. 2005.

17. Gee, K. L., Gabrielson, T. B., Atchley, A. A., and Sparrow, V. W. "Preliminary Analysis of Nonlinearity in Military Jet Aircraft Noise Propagation," *AIAA Journal* Vol. 43, No. 6, 2005, pp. 1398-1401.
doi: 10.2514/1.10155

18. Gee, K. L., Neilsen, T. B., and Atchley, A. A. "Skewness and shock formation in laboratory-scale supersonic jet data," *The Journal of the Acoustical Society of America* Vol. 133, No. 6, 2013, pp. EL491-EL497.

19. Fiévet, R., Tinney, C. E., Baars, W. J., and Hamilton, M. F. "Coalescence in the Sound Field of a Laboratory-Scale Supersonic Jet," *AIAA Journal*, 2015, pp. 1-12.
doi: 10.2514/1.J054252

20. James, M. M., Salton, A. R., Downing, J. M., Gee, K. L., Neilsen, T. B., Reichman, B. O., McKinley, R. L., Wall, A. T., and Gallagher, H. L. "Acoustic Emissions from F-35 Aircraft during Ground Run-Up," *AIAA paper* Vol. 2015-2375, 2015.

21. "Methods for the Measurement of Noise Emissions from High Performance Military Jet Aircraft, ANSI S12.75-2012," *AIAA Journal* Vol. 47, No. 1, 2009, pp. 186-194.

22. Gee, K. L., Neilsen, T. B., Downing, J. M., James, M. M., McKinley, R. L., McKinley, R. C., and Wall, A. T. "Near-field shock formation in noise propagation from a high-power jet aircraft," *The Journal of the Acoustical Society of America* Vol. 133, No. 2, 2013, pp. EL88-EL93.

23. , !!! INVALID CITATION !!! .

24. Gee, K. L., Neilsen, T. B., Thomas, D. C., Reichman, B. O., Muhlestein, M., Downing, J. M., James, M. M., and McKinley, R. L. "Comparison of two time-domain measures of nonlinearity in near-field propagation of high-power jet noise," *20th AIAA/CEAS Aeroacoustics Conference*. American Institute of Aeronautics and Astronautics, 2014.

25. "Acoustics - Description, measurement and assessment of environmental noise -- Part 1: Basic quantities and assesment procedures," *ISO* Vol. 1996-1:2016, 2016.

26. Baars, W. J. "Acoustics from high-speed jets with crackle," *Aerospace Engineering*. University of Texas at Austin, 2013.

27. Gee, K. L., Atchley, A. A., Falco, L. E., and Shepherd, M. R. "Nonlinearity analysis of model-scale jet noise," *19th International Symposium on Nonlinear Acoustics*. Vol. 1474, AIP Publishing, Tokyo, Japan, 2012, pp. 307-310.
28. Petitjean, B. P., Viswanathan, K., and McLaughlin, D. K. "Acoustic pressure waveforms measured in high speed jet noise experiencing nonlinear propagation," *International Journal of Aeroacoustics* Vol. 5, No. 2, 2006, pp. 193-215.

29. Reichman, B. O., Wall, A. T., Gee, K. L., Neilsen, T. B., Downing, J. M., James, M. M., and McKinley, R. L. "Modeling Far-field Acoustical Nonlinearity from F-35 Aircraft during Ground Run-up," *AIAA paper* Vol. 2016-1888, 2016.

30. Gee, K. L., Sparrow, V. W., James, M. M., Downing, J. M., Hobbs, C. M., Gabrielson, T. B., and Atchley, A. A. "Measurement and prediction of noise propagation from a high-power jet aircraft," *AIAA Journal* Vol. 45, No. 12, 2007, pp. 3003-3006.

31. Lee, S., Morris, P. J., and Brentner, K. S. "Improved Algorithm for Nonlinear Sound Propagation with Aircraft and Helicopter Noise Applications," *AIAA Journal* Vol. 48, No. 11, 2010, pp. 2586-2595.
doi: 10.2514/1.J050396
32. Saxena, S., Morris, P. J., and Viswanathan, K. "Algorithm for the nonlinear propagation of broadband jet noise," *AIAA Journal* Vol. 47, No. 1, 2009, pp. 186-194.

33. Brouwer, H. "Numerical simulation of nonlinear jet noise propagation," *11th AIAA/CEAS Aeroacoustics Conference*. 2005, p. 3088.